SHAPE DISTANCE FOR ROTATION ESTIMATION AND ROTATIONAL SYMMETRY DETECTION IN GRAY-LEVEL IMAGES

Stéphane Derrode† and Faouzi Ghorbel‡

†Institut Fresnel (UMR 6133), GSM, ENSPM
Domaine Universitaire de Saint Jerôme, 13013 Marseille Cedex 20, France
Tel: +33 4 91 288 089; e-mail: stephane.derrode@enspm.u-3mrs.fr

‡Laboratoire Cristal, GRIFT, ENSI
Domaine Universitaire de La Manuba, 2010 Manuba, Tunisia
Tel: +216 1 600 444; e-mail: faouzi.ghorbel@ensi.rnu.tn

ABSTRACT

In this work, the analytical Fourier-Mellin transform (AFMT) is used to derive two algorithms for, first, the estimation of the orientation parameter between two objects with the same shape, and second, the detection of all rotational symmetric axes in gray-level images. These algorithms are based on the computation of the Hausdorff distance between shapes when expressed in the Fourier-Mellin domain. Experiments are conducted on gray-level images, confirming the robustness of the algorithms and the accuracy of the estimated parameters.

1 INTRODUCTION

The Fourier-Mellin transform has been extensively studied for pattern description and recognition in the last decades. A number of works to date were motivated by the search for some sets of features invariant under rotation and scale transformations [11]. Due to the crucial numerical problem faced in estimating the standard FMT, the analytical Fourier-Mellin transform (AFMT) was proposed in [5] and three efficient approximations were then presented [3]. In this work, the AFMT is used to derive two algorithms for, first, the estimation of the orientation parameter between two objects with the same shape, and second, the detection of all rotational symmetric axes in gray-level images.

From results on commutative harmonic analysis for the group of similarities (as the direct product of the rotation and scale groups), i.e. shift theorem and Parseval equality, we show that the shape of an object is an equivalence class of similar objects up to a similarity transformation. When the group of transformations is restricted to the compact group of rotations, the natural distance in the shape space becomes the Hausdorff one. This result extends the one obtained on closed contours and Fourier coefficients [2] to gray-level objects and AFMT.

This interesting result is first used to derive an algorithm for the estimation of the orientation parameter between two similar objects. The correspondance problem between images is solved simultaneously according to the Hausdorff distance value. The approach proposed is related to global image registration algorithms, such as correlation and matching filters [7, 1], and needs neither invariant descriptors, nor matching primitives, but works directly on gray-level objects.

Finally, by computing the Hausdorff between an image and itself in the AFMT domain, we were able to derive another algorithm for the detection and localization of all the rotational symmetry axes in gray-level images. The method is similar to some extent to the work proposed by D. Shen et al in [9], in the case of reflectional symmetry and complex moments.

This paper is organized as follows. The AFMT and some of its relevant properties are presented in section 2. Section 3 presents the main result regarding the computation of the Hausdorff distance between shapes in the AFMT domain. In section 4, we then derive an algorithm for the detection of all rotational symmetries of any gray-level image. Experimental result on gray-level images are presented.

2 FORMULATION

Throughout this paper, we shall denote by $\mathbb{Z}$ the additive group of integers, $\mathbb{R}$ the additive group of the real line, $\mathbb{R}_+^*$ the multiplicative group of positive and non-zero real numbers and $\mathbb{S}^1$ the unit circle of the plane $\mathbb{R}^2$. All these groups are locally compact and commutative. The direct product $\mathcal{G} = \mathbb{R}_+^* \times \mathbb{S}^1$ forms a locally compact and commutative group under the following law : $(\alpha, \theta) \circ (\rho, \psi) = (\alpha\rho, \theta + \psi)$. $\mathcal{G}$ is formed by all planar and positive similarities centered on the origin of axes and is equivalent to the polar coordinate space.

2.1 The analytical FM transform

We denote by $\mathbf{L}^p(\mathcal{G})$ the normed vector spaces of integrable ($p=1$) and square integrable ($p=2$) real valued functions defined on $\mathcal{G}$: $f \in \mathbf{L}^p(\mathcal{G}) \Leftrightarrow$

$$\|f\|_{\mathbf{L}^p(\mathcal{G})} = \left(\int_0^\infty \int_0^{2\pi} |f(r,\theta)|^p \; d\theta \frac{dr}{r} \right)^{\frac{1}{p}} < \infty. \quad (1)$$

The Fourier-Mellin Transform (FMT) is defined for functions in $\mathbf{L}^1(\mathcal{G})$. However, in general, gray-scale images cannot be assimilated to such functions and it was proposed to compute the FMT of $f_\sigma(r,\theta) = r^\sigma f(r,\theta)$ with $\sigma > 0$ [5]. The FMT of f_σ is called the Analytical Fourier-Mellin Transform (AFMT) of f and can be written in this way: $\forall (k,v) \in \hat{\mathcal{G}}$,

$$\mathcal{M}_{f_\sigma}(k,v) = \frac{1}{2\pi} \int_0^\infty \int_0^{2\pi} f(r,\theta)\, r^{\sigma - iv}\, e^{-ik\theta}\, d\theta \frac{dr}{r}, \quad (2)$$

where $\hat{\mathcal{G}} = \mathbb{Z} \times \mathbb{R}$ is the dual group of $\mathcal{G}$ [4] and represents the parameters space in the Fourier-Mellin domain. The AFMT can be seen as the Laplace transform on the planar similarity group. It gives a unique description and images can be retrieved with the inverse AFMT [3].

2.2 Parseval equality

We denote by $\mathbf{L}^2(\hat{\mathcal{G}})$, the space of square integrable complex valued functions defined on $\hat{\mathcal{G}}$: $h \in \mathbf{L}^2(\hat{\mathcal{G}}) \Leftrightarrow$

$$\|h\|_{\mathbf{L}^2(\hat{\mathcal{G}})} = \left(\int_{-\infty}^{+\infty} \sum_{k \in \mathbb{Z}} |h(k,v)|^2 \, dv \right)^{\frac{1}{2}} < \infty. \quad (3)$$

The Plancherel theorem can be extended to every locally compact and commutative group [8]. For f_σ in $\mathbf{L}^1(\mathcal{G}) \cap \mathbf{L}^2(\mathcal{G})$, $\mathcal{M}_{f_\sigma} \in \mathbf{L}^2(\hat{\mathcal{G}})$ and the Parseval equality is given by :

$$\|f_\sigma\|_{\mathbf{L}^2(\mathcal{G})} = \|\mathcal{M}_{f_\sigma}\|_{\mathbf{L}^2(\hat{\mathcal{G}})}. \quad (4)$$

In what follows, we assume that a gray-level object is represented by a function $f_\sigma \in \mathbf{L}^1(\mathcal{G}) \cap \mathbf{L}^2(\mathcal{G})$ (original description) or, in a strictly equivalent way, by its FMT $\mathcal{M}_{f_\sigma} \in \mathbf{L}^2(\hat{\mathcal{G}})$ (dual Fourier-Mellin description).

2.3 Gray-level shape

An object retains its shape whatever its position in the image. So, the notion of shape is directly connected to a group of transformations. In the case of gray-level images and similarity transformations, shapes can be characterized efficiently by the AFMT using an appropriate shift theorem.

Let f^2 denote the rotation and size change of an object f^1 through angle $\beta \in \mathbb{S}^1$ and scale factor $\alpha \in \mathbb{R}_+^*$, i.e. $f^2(r,\theta) = f^1(\alpha r, \theta + \beta)$. Two such objects will be termed similar objects. It is easy to show that their AFMT are related according to: $\forall (k,v) \in \hat{\mathcal{G}}$,

$$\mathcal{M}_{f^2_\sigma}(k,v) = \alpha^{-\sigma+iv}\, e^{ik\beta}\, \mathcal{M}_{f^1_\sigma}(k,v). \quad (5)$$

These relations can be seen as the shift theorem for the planar and positive similarity group. Going through the group of positive similarities, the shape $\mathbb{F}$ of an object f could be defined as the set of all similar objects according to $\mathcal{G}$:

$$\mathbb{F} = \left\{ \Big(f\left(\alpha r, \theta + \beta\right) \Big), (\alpha, \beta) \in \mathbb{R}_+^* \times \mathbb{S}^1 \right\}, \quad (6)$$

and, using Eq. (4) and (5), a shape is also defined in a strictly equivalent way in the Fourier-Mellin domain by:

$$\mathbb{F} = \left\{ \left(\alpha^{-\sigma+iv} e^{ik\beta} \mathcal{M}_{f_\sigma}(k,v) \right), (\alpha,\beta) \in \mathbb{R}_+^* \times \mathbb{S}^1 \right\}. \quad (7)$$

It can be shown that a shape is an equivalence class through the action of $\mathcal{G}$ [6]. However such a class is not compact since $\mathbb{R}_+^*$ is not. When considering only the group of rotations, shapes become compact sets and the Hausdorff distance is the natural metric on the shape space.

3 Hausdorff distance in the FM domain

If the set of transformations is restricted to the one parameter plane rotation group $\mathbb{S}^1$, a shape is formed by all similar objects up to a rotation. In the FM domain, we get from Eq. (7), setting $\alpha = 1$:

$$\mathbb{F} = \left\{ \left(e^{ik\beta}\, \mathcal{M}_{f_\sigma}(k,v) \right)_{(k,v) \in \hat{\mathcal{G}}}, \beta \in \mathbb{S}^1 \right\}.$$

Shapes are now compact and bounded sets since there exists a continuous bijection with $\mathbb{S}^1$. The shape space becomes the quotient space $\mathbf{L}^2(\mathbb{Z} \times \mathbb{R})/\mathbb{S}^1$ which is a metric space with the Hausdorff distance [4, 6]. The Hausdorff distance Δ between two shapes $\mathbb{F}$ and $\mathbb{G}$ is given by:

$$\Delta(\mathbb{F},\mathbb{G}) = \max\left(\delta(\mathbb{F},\mathbb{G}), \delta(\mathbb{G},\mathbb{F})\right),$$
$$\delta(\mathbb{F},\mathbb{G}) = \max_{f \in \mathbb{F}} \min_{g \in \mathbb{G}} d_2(f,g),$$

where d_2 is the Euclidean distance derived from the $\mathbf{L}^2$-norms. In the FM domain, we get:

$$\begin{aligned} \delta(\mathbb{F},\mathbb{G}) &= \max_{\varphi \in \mathbb{S}^1} \min_{\phi \in \mathbb{S}^1} \left\| e^{ik\varphi} \mathcal{M}_{f_\sigma}(k,v) - e^{ik\phi} \mathcal{M}_{g_\sigma}(k,v) \right\|, \\ &= \max_{\varphi \in \mathbb{S}^1} \min_{\phi \in \mathbb{S}^1} \left\| \mathcal{M}_{f_\sigma}(k,v) - e^{ik(\phi-\varphi)} \mathcal{M}_{g_\sigma}(k,v) \right\|. \end{aligned}$$

Using the change of variable $\psi = \phi - \varphi$, we get $\delta(\mathbb{F},\mathbb{G}) = \min_{\psi \in \mathbb{S}^1} \mathbf{E}_{f_\sigma, g_\sigma}(\psi)$ with :

$$\mathbf{E}_{f_\sigma, g_\sigma}(\psi) = \left(\int_{-\infty}^{+\infty} \sum_{k \in \mathbb{Z}} \left| \mathcal{M}_{f_\sigma}(k,v) - e^{ik\psi}\, \mathcal{M}_{g_\sigma}(k,v) \right|^2 dv \right)^{\frac{1}{2}}. \quad (8)$$

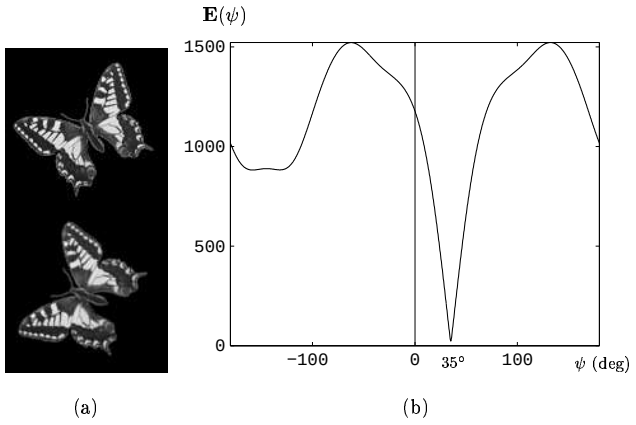

Figure 1: Plot of the Hausdorff distance (b) computed from the two images in (a). The minimum value $\Delta = 23.61$ is attained for $\psi = 35.02°$.

In a similar way, we also get $\delta(\mathbb{G}, \mathbb{F}) = \min_{\psi \in \mathbb{S}^1} \mathbf{E}_{g_\sigma, f_\sigma}(\psi) = \min_{\psi \in \mathbb{S}^1} \mathbf{E}_{f_\sigma, g_\sigma}(\psi)$, and the Hausdorff distance is reduced to the following quantity :

$$\Delta(\mathbb{F}, \mathbb{G}) = \min_{\psi \in \mathbb{S}^1} \mathbf{E}_{f_\sigma, g_\sigma}(\psi). \tag{9}$$

This result ensures the uniqueness of parameters and extends the one obtained on closed contours and Fourier coefficients [2] to gray-level images and AFMT. It is the basis for the rotational symmetry detection algorithm presented in the next section.

For illustration purposes, figure 1 shows the Hausdorff distance computed from the two gray-level images of a butterfly. The minimum value, obtained by an optimization method, is attained for $\psi = 35°$ which is precisely the orientation difference between the two images. Note that Δ is not exactly zero due to the numerical approximations in estimating (9) and the anisotropy of the Cartesian grid.

4 Application to rotational symmetry estimation

From the result presented above, an algorithm is now derived for the detection and estimation of rotational symmetries in gray-level images. Experimental results are conducted on the four test images in Fig. 2. Images (a) and (b) show 9 and 3 rotation and reflection symmetries respectively. The image in (c) represents a special case of an image with an 'infinite number' of both symmetry types. The last image (d) presents one reflection and no rotation symmetry.

Following [10], a 2D image is called P rotationally symmetric (P-RSI for short), if it is invariant under rotation of $2\pi/\mathrm{P}$ about the center of mass of the object

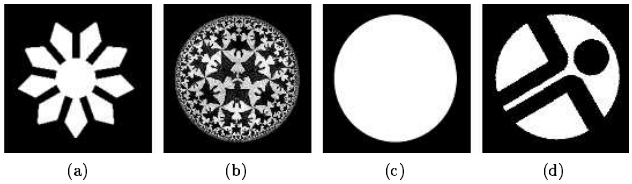

Figure 2: Four test images used for symmetry estimation experiments. Image (b) contains 190 gray levels. Image (d) comes from the Image Computing Group, City University of Hong Kong.

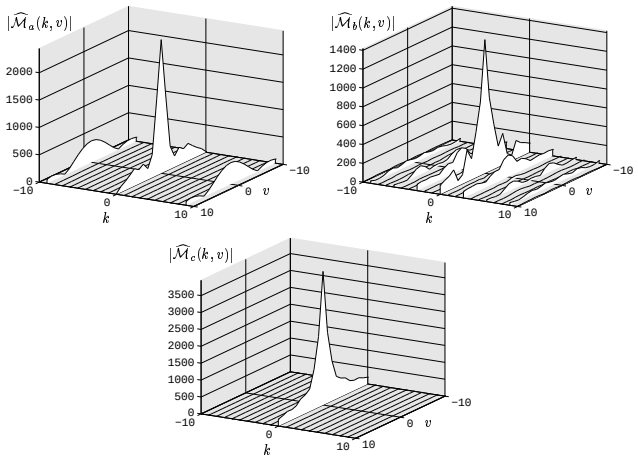

Figure 3: Magnitude of central Fourier-Mellin harmonics of the RSIs (a), (b) and (c) in Fig. 2.

and P is the largest integer: $\forall (r, \theta) \in \mathbb{R}_+^* \times \mathbb{S}^1$,

$$f(r, \theta) = f\left(r, \theta + \frac{2\pi l}{\mathrm{P}}\right), \quad l = 0, \ldots, \mathrm{P} - 1. \tag{10}$$

The AFMT can be seen as the analytical Mellin transform of the Fourier coefficients of an image. Since the Fourier coefficients $\mathcal{F}(k)$ of a P-RSI f is zero for every k not a multiple of P, the AFMT is zero except for k multiple of P and v real. This is illustrated in Fig. 3 which shows the magnitude of central Fourier-Mellin harmonics of the three RSIs in Fig. 2. In the first two cases, the AFMT is zero for k a multiple of 9 and 3 respectively, which corresponds to the number of fold axes in the images. In the case of the disk, the FMT is zero except for $k = 0$ and corresponds to the special case of an image with an 'infinite number' of folds.

For the detection and estimation of folds in an RSI f, we propose to compute $\mathbf{E}_{f_\sigma, f_\sigma}(\psi)$ from (8), which can be written as: $\forall \psi \in \mathbb{S}^1$,

$$\mathbf{E}_{f_\sigma, f_\sigma}(\psi) = \left(2 \sum_{k \in \mathbb{Z}} (1 - \cos(k\psi)) \int_{-\infty}^{+\infty} |\mathcal{M}_{f_\sigma}(k, v)|^2 \, dv\right)^{\frac{1}{2}}. \tag{11}$$

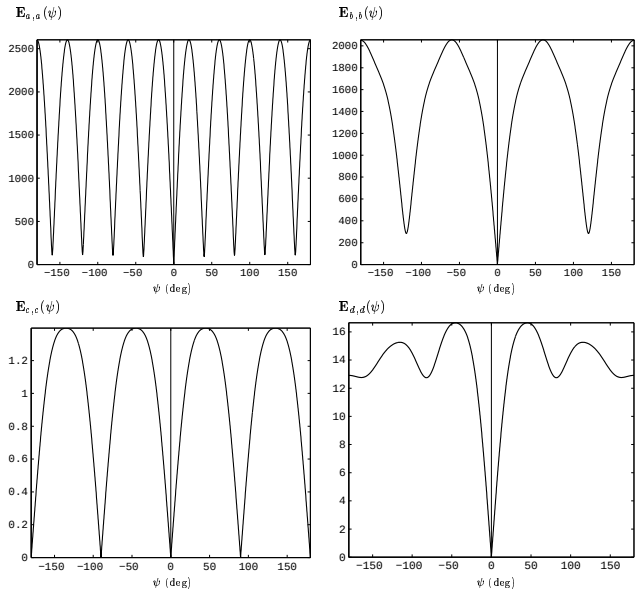

Figure 4: Plot of $\mathbf{E}_{f_\sigma,f_\sigma}(\psi)$ for the four images in Fig. 2.

It is easy to show that $\mathbf{E}_{f_\sigma,f_\sigma}$ is even and periodic with period $\frac{2\pi}{\mathrm{P}}$. The orientation of the folds is given by angles ψ_i such that $\mathbf{E}_{f_\sigma,f_\sigma}(\psi_i) = 0$. The solution $\mathbf{E}_{f_\sigma,f_\sigma}(0) = 0$ is always true since any image is rotationally symmetric with respect to 0° rotation.

The detected axes for the shapes sketched in figure 2 are reported in figure 4. Angles are given from the x-axis and clockwise. The top-left result shows nearly zero values according to the fold axes of image 2(a). The minima of the top-right result correspond to the rotation symmetric axes (−120°, 0° and 120°). For the disk image (bottom-left result), $\mathbf{E}$ should have been exactly zero everywhere, which is not the case, due to approximations. We only get exactly zero for angles that are multiples of 90° since the Cartesian grid is isotropic to these angles (every pixel finds an exact location on the grid). Nevertheless, the curve is near zero compared to other results. The last image (bottom-right) is not rotationally symmetric and the only zero is located at $\psi = 0$.

5 Conclusion

The problem of estimating the rotation parameter between two gray-level objects has been formulated as the computation of the Hausdorff distance between shapes when expressed in the Fourier-Mellin domain. This result ensures the uniqueness of parameters and extends the result obtained in [2] for planar closed contours and Fourier coefficients to gray-level images and AFMT. As an application, the Hausdorff distance has then been used in order to detect and localize all the rotational symmetry axes in gray-level object. One advantage is that we do not assume the image to be symmetric since the localization of the minima can be used to determine whether the input image is symmetric or not. The experimental results confirm the robustness of the algorithms and the accuracy of the estimated parameters. The extension of the algorithm to reflectional symmetry appears to be rather straightforward.

References

[1] L. Benyoussef, Y. Delignon, and F. Ghorbel. An optimal matched filter for target detection in images distorted by noise. In *Proc. of the Int. Conf. on Geoscience and Remote Sensing*, volume 2, pages 1001–1003, Seatle (USA), 6-10 July 1998.

[2] M. Daoudi et al. Shape distances for contour tracking and motion estimation. *Pattern Recognition*, 32:1297–1306, 1999.

[3] S. Derrode and F. Ghorbel. Robust and efficient Fourier-Mellin transform approximations for gray-level image reconstruction and complete invariant description. *Computer Vision and Image Understanding*, 83(1):57–78, 2001.

[4] J. Dieudonné. *Éléments d'analyse.* Tome II. Gauthier-Villars, Cahiers scientifiques, Paris (Fr.), 1983.

[5] F. Ghorbel. A complete invariant description for gray-level images by the harmonic analysis approach. *Pattern Recognition Letters*, 15:1043–1051, 1994.

[6] F. Ghorbel. Towards a unitary formulation for invariant image description; Application to image coding. *Ann. Telecom.*, 53(3):143–153, 1998.

[7] D. Huttenlocher and S. Ullman. Recognizing solid objects by alignement with an image. *Int. J. of Computer Vision*, 5(2):195–212, 1990.

[8] W. Rudin. *Fourier analysis on groups.* Wiley Classics, New York, 1990.

[9] D. Shen, H. Ip, and E. Teoh. An energy of asymmetry for accurate detection of global reflection axes. *Image and Vision Computing*, 19:283–297, 2001.

[10] D. Shen et al. Symmetry detection by generalized complex (GC) moments: A close-form solution. *IEEE trans. on PAMI*, 21(5):466–475, 1999.

[11] Y. Sheng and H. Arsenault. Experiments on pattern recognition using invariant Fourier-Mellin descriptors. *J. of the OSA A*, 3(6):771–776, 1986.